Visualizing odorant receptor trafficking in living cells down to the single-molecule level

V. Jacquier, M. Prummer, J.-M. Segura, H. Pick, and H. Vogel*

Institute of Chemical Sciences and Engineering (ISIC), Ecole Polytechnique Fédérale de Lausanne (EPFL), CH-1015 Lausanne, Switzerland

Edited by H. Ronald Kaback, University of California, Los Angeles, CA, and approved July 25, 2006 (received for review May 17, 2006)

Despite the importance of trafficking for regulating G protein-coupled receptor signaling, for many members of the seven transmembrane helix protein family, such as odorant receptors, little is known about this process in live cells. Here, the complete life cycle of the human odorant receptor OR17-40 was directly monitored in living cells by ensemble and single-molecule imaging, using a double-labeling strategy. While the overall, intracellular trafficking of the receptor was visualized continuously by using a GFP tag, selective imaging of cell surface receptors was achieved by pulse-labeling an acyl carrier protein tag. We found that OR17-40 efficiently translocated to the plasma membrane only at low expression, whereas at higher biosynthesis the receptor accumulated in intracellular compartments. Receptors in the plasma membrane showed high turnover resulting from constitutive internalization along the clathrin pathway, even in the absence of ligand. Single-molecule microscopy allowed monitoring of the early, dynamic processes in odorant receptor signaling. Although mobile receptors initially diffused either freely or within domains of various sizes, binding of an agonist or an antagonist increased partitioning of receptors into small domains of ≈190 nm, which likely are precursors of clathrin-coated pits. The binding of a ligand, therefore, resulted in modulation of the continuous, constitutive internalization. After endocytosis, receptors were directed to early endosomes for recycling. This unique mechanism of continuous internalization and recycling of OR17-40 might be instrumental in allowing rapid recovery of odor perception.

cell signaling | G protein-coupled receptors | single-particle tracking | *in vivo* protein labeling | fluorescence imaging

The sensation of smell is mediated by a specific family of olfactory G protein-coupled receptors (GPCRs), which recognize small volatile molecules (1). Although odorant receptors (ORs) account for the largest mammalian gene family, comprising up to 1,000 members, the mechanism of signal recognition and amplification in olfactory transduction remains elusive (2). This is partly because classical methods for OR detection, based on immunocytochemistry (3, 4) or genetic fusion to GFP (5), have not permitted the simultaneous live-cell imaging of olfactory processes at the cell membrane and in cytoplasmic compartments.

Comprehensive functional studies on ORs in a native cellular environment, such as isolated olfactory sensory neurons, adenovirus-infected olfactory epithelia, or genetically engineered animals, are often hampered by practical limitations: (*i*) olfactory sensory neurons are difficult to maintain in primary culture (6), (*ii*) virus-mediated gene transfer does not consistently yield functional OR expression (7), and (*iii*) creating transgenic animals for each OR would be quite expensive. Functional expression of ORs in heterologous cells is, therefore, an important approach for elucidating the molecular mechanism of olfaction and helps to identify specific ligands for particular receptors. Unfortunately, ORs express very inefficiently at the plasma membrane of heterologous cells, apparently because of OR retention in intracellular compartments and degradation via the ubiquitin–proteasome pathway (8–10). However, direct monitoring of these processes *in vivo* is still immature. Such monitoring would be facilitated by the development of generic fluorescence labeling approaches for real-time observation of ORs in living cells. Monitoring different stages of OR expression, trafficking, and turnover can provide valuable information for manipulating these processes *in vivo* and open possibilities for improving heterologous expression and elucidating cellular signaling reactions.

In the present article, we focus on the functional properties and spatiotemporal distribution of the human odorant receptor OR17-40 (11) in living cells by using two complementary fluorescence labeling methods: (*i*) genetic fusion of GFP at the intracellular C terminus of the OR and (*ii*) posttranslational *in vivo* labeling of an N-terminal extension encoding the *Escherichia coli* acyl carrier protein (ACP). A fluorophore can be covalently transferred to the ACP tag by phosphopantetheine transferase (PPTase) from a fluorescent CoA derivative (12). This orthogonal labeling approach allowed the resolution of sequential stages of biogenesis and trafficking of an olfactory GPCR. The fluorescent tags did not interfere with biological function and enabled us not only to visualize receptor biosynthesis in intracellular compartments, but also to optically distinguish and quantitatively compare surface (ACP-labeled) and total (GFP-tagged) receptor pools at any time in living cells. Because the small fluorophore added by ACP labeling does not prevent receptor endocytosis, we could reveal constitutive receptor internalization in the absence of an agonist. With the same approach, we recently quantified the membrane distribution of a prototypical GPCR with great precision (13).

Moreover, ACP labeling allowed us to image the complex mobility pattern of single OR molecules in the cell membrane. During the first steps of the signaling cascade, ORs redistributed from a major freely or weakly confined diffusing population to a more strongly confined fraction and an immobile fraction, reflecting transfer to clathrin-coated pits. Surprisingly, this slowdown and confinement was similar for both ligand types, albeit more pronounced for the antagonist.

Results

Fluorescence Double-Labeling of OR17-40. HEK293 cells stably expressing ACP-OR17-40 (Fig. 1*A*) or ACP-OR17-40-GFP (Fig. 1*B*) were investigated by confocal microscopy. The N-terminal ACP tag located at the extracellular part of the receptor allowed specific fluorescence pulse labeling of plasma-membrane-inserted receptors (12, 13), as shown in Fig. 1*C*. To continuously monitor all translated receptors and their subcellular localization, GFP was fused to the intracellular C-terminal part of OR17-40. Based on the dual-color visualization enabled by combined receptor tagging with ACP and GFP, the population of functionally integrated surface

Author contributions: V.J., M.P., J.-M.S., H.P., and H.V. designed research; V.J., M.P., and H.P. performed research; V.J., M.P., and H.P. analyzed data; and V.J., M.P., J.-M.S., H.P., and H.V. wrote the paper.

The authors declare no conflict of interest.

This paper was submitted directly (Track II) to the PNAS office.

Abbreviations: ACP, acyl carrier protein; AMCA, α-methyl-cinnamaldehyde; ECFP, enhanced cyan fluorescent protein; ER, endoplasmic reticulum; GPCR, G protein-coupled receptor; OR, odorant receptor.

*To whom correspondence should be addressed. E-mail: horst.vogel@epfl.ch.

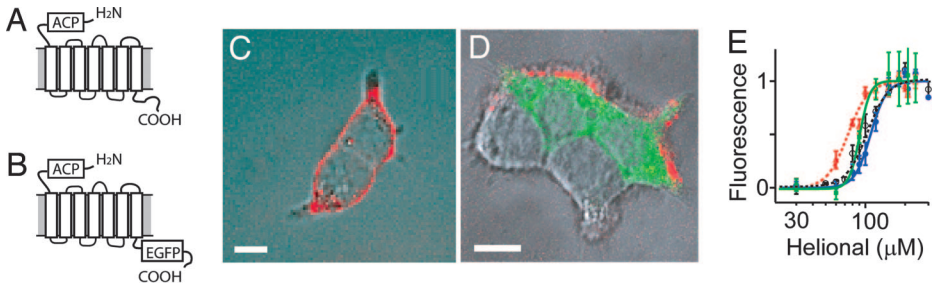

Fig. 1. Subcellular localization and functional characterization of ORs. (*A* and *B*) Model of ACP-OR17-40 (*A*) and ACP-OR17-40-GFP (*B*) showing the seven transmembrane helices and the different C- and N-terminal modifications. (*C*) Membrane localization of Cy5-ACP-OR17-40. (*D*) Localization of the total Cy5-ACP-OR17-40-GFP population (green) and the membrane-resident fraction (red). (*E*) Helional dose [Ca^{2+}] response of ACP-OR17-40 (blue), ACP-OR17-40-GFP (green), and labeled ACP-OR17-40 (red) in the presence of $G_{\alpha q}$. OR-mediated intracellular [Ca^{2+}] responses were measured as described in ref. 11. (Scale bars: 10 μm.)

receptors could be related to the overall receptor expression in individual cells (Fig. 1*D*). Only a limited number of the translated ORs translocated to the plasma membrane; most of them were trapped in intracellular membranes. Remarkably, low-expressing cells (low GFP signal) exhibited a higher number of receptors at the plasma membrane, as revealed by an increased Cy5 signal at the cell surface (11).

To probe the functionality of the fusion constructs, we performed calcium imaging on cells expressing either ACP-OR17-40 or ACP-OR17-40-GFP together with a promiscuous $G_{\alpha q}$ protein. Both fusion constructs elicited a dose-dependent Ca^{2+} response after application of helional (Fig. 1*E*), with EC_{50}s (mean ± 95% confidence interval) of 108.0 ± 9.0 μM for ACP-OR17-40 and 90.7 ± 18.2 μM for ACP-OR17-40-GFP, both consistent with the EC_{50} of the wild type (98.7 ± 9.6 μM). Furthermore, the receptor was still functional after labeling with CoA–Cy5 (EC_{50} = 73.7 ± 8.3 μM).

Biogenesis and Membrane Trafficking. The evolution of the average expression of ACP-OR17-40-GFP in the whole cell population was analyzed by FACS. Labeling with CoA–Cy5 allowed us to monitor only the receptors reaching the plasma membrane; the GFP signal quantifies the total number of translated receptors. The total receptor expression reached a plateau ≈27 h after transfection, and the time course of membrane insertion was delayed by 4–5 h (Fig. 2*A*). The fluorescence signal at the membrane was detectable only in low-expressing cells, indicating that OR membrane insertion was improved.

Typically, 4 h after transfection the first signal from ACP-OR17-40-GFP was detected in the endoplasmic reticulum (ER). The subcellular localization of the receptor was determined by overlapping the GFP fluorescence with a spectrally distinguishable, cotransfected enhanced cyan fluorescent protein (ECFP)-ER marker (Fig. 2*B*). The first ORs reached the Golgi apparatus 0.5–1 h later, as revealed with cotransfected ECFP-Golgi marker (Fig. 2*C*). Surprisingly, the receptor translocation from the ER to the Golgi apparatus was observed only in low-expressing cells. At high expression levels, the receptor accumulated in the ER without progress (Fig. 2*D*) for at least 24 h after transfection. In contrast, in low-expressing cells the receptor was already detected at the cell surface 7–8 h after transfection (Fig. 2*E*). The punctuated distribution of OR17-40 in the plasma membrane is similar to what has been reported for other ORs (8, 14) and suggests receptor clustering. At ≈30 min after ACP labeling, the punctuated pattern on the cell surface gave rise to cytosolic bright spots (Fig. 2*F*), which we assign to intracellular vesicles.

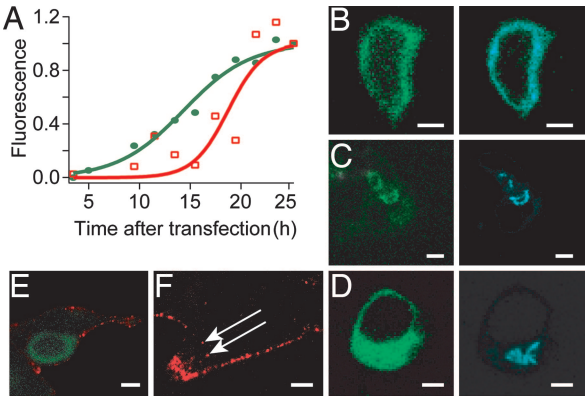

Fig. 2. Biogenesis and membrane trafficking. (*A*) Time-lapse analysis of ACP-OR17-40-GFP expression by FACS: normalized total expression (filled circles, GFP) and membrane-resident fraction (open squares, Cy5). Lines were added to guide the eye. (*B–D*) Confocal images of ACP-OR17-40-GFP (*Left*) and several ECFP organelle markers (*Right*) at different time points after transfection. After 4–5 h (*B*), the receptor colocalizes with an ER marker. At ≈30 min later (*C*), the OR colocalizes with a Golgi marker in low-expressing cells. Even after ≈8 h (*D*), the OR does not colocalize with a Golgi marker in high-expressing cells. (*E*) At 7–8 h after transfection, part of the OR population (green) can be seen at the plasma membrane in low-expressing cells after labeling with CoA–Cy5 (red). (*F*) At ≈30 min after labeling, intracellular vesicles (indicated by arrows) appeared inside the cells. (Scale bars: 5 μm.)

Constitutive Internalization of OR17-40. To confirm that the bright spots in Fig. 2*F* were indeed intracellular vesicles, we labeled ACP-OR17-40 with CoA–CypHer, which is nonfluorescent at neutral pH and highly fluorescent when protonated in intracellular acidic vesicles (15). At 15–30 min after labeling, CypHer fluorescence was high and concentrated in vesicles that were moving below the plasma membrane (Fig. 3*A*). Because ACP labeling targets only cell surface receptors, the intracellular fluorescent vesicles must arise from internalized receptors. Labeling of GPCRs by the ACP method does not induce endocytosis, as shown for the neurokinin-1 receptor (16).

To characterize the pathway by which OR17-40 constitutively internalizes, we incubated the cells with hypertonic sucrose, which is known to selectively inhibit clathrin-mediated endocytosis by reducing the number of clathrin-coated pits (17). When cells expressing ACP-OR17-40 were incubated in 0.45 M sucrose 10 min before and during labeling with CoA–CypHer, the resulting fluorescence was low, homogeneous, and located exclusively at the cell membrane (Fig. 3*B*), in contrast with the nontreated control (Fig. 3*A*). After sucrose removal, rapidly moving vesicles appeared within minutes. Addition of 100–200 μM helional did not induce any detectable receptor internalization, suggesting that both constitutive and agonist-induced internalization occur along the clathrin-mediated pathway. In agreement with these results, internalized CypHer-labeled ORs colocalized in intracellular vesicles with clathrin-GFP, both with and without agonist (Fig. 3*D*).

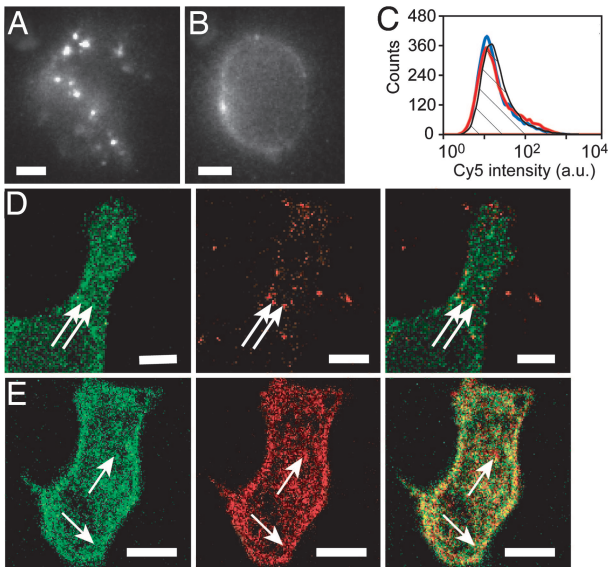

Fig. 3. Constitutive internalization of OR17-40 along the clathrin pathway. (*A*) CypHer-labeled ACP-OR17-40-containing cell with highly fluorescent intracellular vesicles located below the plasma membrane, indicating that the receptor constitutively internalizes. (*B*) Constitutive internalization of CypHer-labeled ACP-OR17-40 is blocked by hypertonic sucrose. (*C*) Constant number of cell surface ORs before and after ligand binding. Cy5 fluorescence of ≈15,000 cells expressing ACP-OR17-40-GFP and labeled with CoA–Cy5 before (black) and after incubation with agonist (red) or antagonist (blue). (*D*) Internalized CypHer-labeled ACP-OR17-40 (red) and GFP-clathrin (green). Colocalization of the two proteins is shown in yellow in the merged image (*Right*). Cells were incubated at 37°C for 20 min after ACP labeling at room temperature. (*E*) Internalized CypHer-labeled ACP-OR17-40 (red) and transferrin-Alexa488 (green) receptors. Colocalization of the two receptors is shown in yellow in the merged image (*Right*). Tf-Alexa488 (50 μg/ml) was added to the cells during ACP labeling at room temperature. Cells were then washed 3× with PBS and incubated at 37°C for 30 min. (Scale bars: 5 μm.)

To identify the organelles containing the internalized ACP-OR17-40, we applied transferrin-Alexa488 (Tf-Alexa488) to the cells. The transferrin receptor is a commonly used marker for endosomes involved in protein sorting and recycling (18–21). CypHer-labeled ORs were present mostly in vesicles containing the transferrin receptor after 30 min incubation at 37°C (Fig. 3*E*), indicating that OR17-40 was localized in early or recycling endosomes after that time. The overlap of the two fluorescent signals increased over time. Cells incubated with 200 μM helional for up to 1 h showed a similar distribution of intracellular vesicles containing both OR and transferrin receptor (data not shown).

The influence of agonist or antagonist binding on receptor internalization was investigated on cells transiently expressing ACP-OR17-40-GFP. Samples were treated for 15 min and 1 h with 200 μM helional or overnight with 300 μM α-methyl-cinnamaldehyde (AMCA). Subsequent labeling with CoA–Cy5 and FACS analysis showed that the number of cell surface receptors did not change under the various conditions (Fig. 3*C*).

Heterogeneous Diffusion of Single OR17-40s. The finding that the number of receptors at the cell surface remained constant even after agonist application might be the result either of the absence of agonist-induced internalization or of a fast recycling so that the population of cell surface receptors had been replenished within the time frame of the FACS experiment. To resolve this problem, we investigated early events of receptor dynamics following agonist application. We used single-molecule microscopy to monitor the diffusion of single OR17-40s in the plasma membrane and their immobilization inside clathrin-coated pits. ACP labeling enabled us to covalently tag a small fraction of the cell surface ORs with the photostable dye Cy5 (Fig. 4 *A* and *B*).

We first investigated the lateral diffusion of OR17-40 in its basal state, which was remarkably heterogeneous. Visual inspection of the recorded trajectories revealed at least four major populations of receptors. Although few receptors diffused freely in the cell membrane and some were immobile, the majority diffused within either large or small domains (Fig. 4 *C* and *D*). We analyzed the dependence of the mean square displacement on the time lag of each single molecule by using the model of confined diffusion and nonlinear least-square fitting. For each trajectory, we determined the domain size L in which the molecule was apparently confined and its diffusion coefficient D.

Without ligand, the distribution of the compartment sizes L was broad and heterogeneous, ranging from 50 nm to several microns (Fig. 5*A*, black). The majority of ORs were found to diffuse confined within domains of ≈300 nm in size. To go further, we would argue (with some reservation, which will be resolved in *Ligand-Induced Confinement of OR17-40s in Small Domains*, below) that $P(L)$ might comprise at least two additional, potentially significant confined subpopulations peaked at ≈190 nm and ≈550 nm. Finally, molecules were considered immobile if $L < 120$ nm, which corresponds to the experimental localization uncertainty limited by the photon counts per frame. The diffusion coefficient D was distributed over several orders of magnitude, $2 \times 10^{-3} \leq D \leq 1 \times 10^{-1}$ μm²/s (Fig. 5*B*, black), with a single peak at ≈0.02 μm²/s.

Both the diffusion coefficient and the confinement size derived from single-particle tracking can contain systematic errors due to the finite integration time of the camera used for recording (22). Taking into account typical measured values, $L_m = 0.2$ μm and $D_m = 0.02$ μm²/s, we underestimate L_{true} and D_{true} typically by 10% and 20%, respectively.

To simplify the picture, we can sort the trajectories into four classes (Fig. 5*C*): (*i*) immobile molecules with $0 < L < 0.12$ μm, (*ii*) freely diffusing molecules with $L > 1$ μm, (*iii*) molecules confined in small domains with $0.12 < L < 0.25$ μm, and (*iv*) molecules confined in large domains with $0.25 < L < 1$ μm. The separation

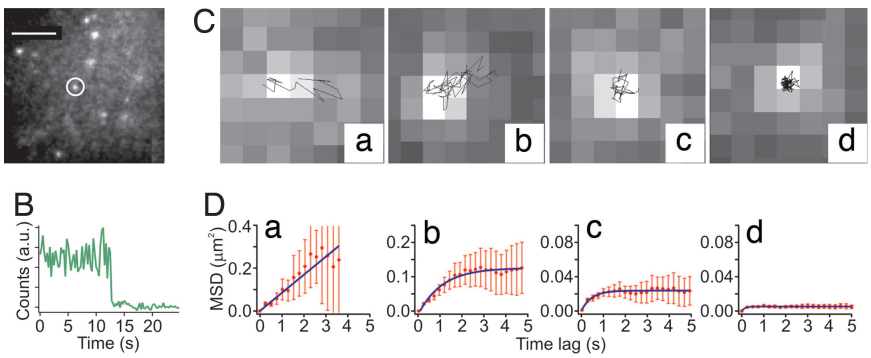

Fig. 4. Lateral diffusion of ORs. (*A*) Fluorescence image of Cy5-labeled ACP-OR17-40 receptors in a single HEK293 cell. (Scale bar: 5 μm.) (*B*) Fluorescence time trace of the receptor marked in *A*, showing the characteristic single-step photobleaching. (*C*) Diffusion modes of single ORs, shown for four typical trajectories superimposed on the OR fluorescence images (pixel size: 225 nm). (*D*) MSD(t_{lag}) of the trajectories in *C*. Solid lines represent the fit of the data according to free Brownian motion (*a*) and confined diffusion (*b–d*). Note that the vertical scale changes. At least four different mobility classes are found: free diffusion (*a*), weak confinement (*b*), strong confinement (*c*), and immobile molecules (*d*).

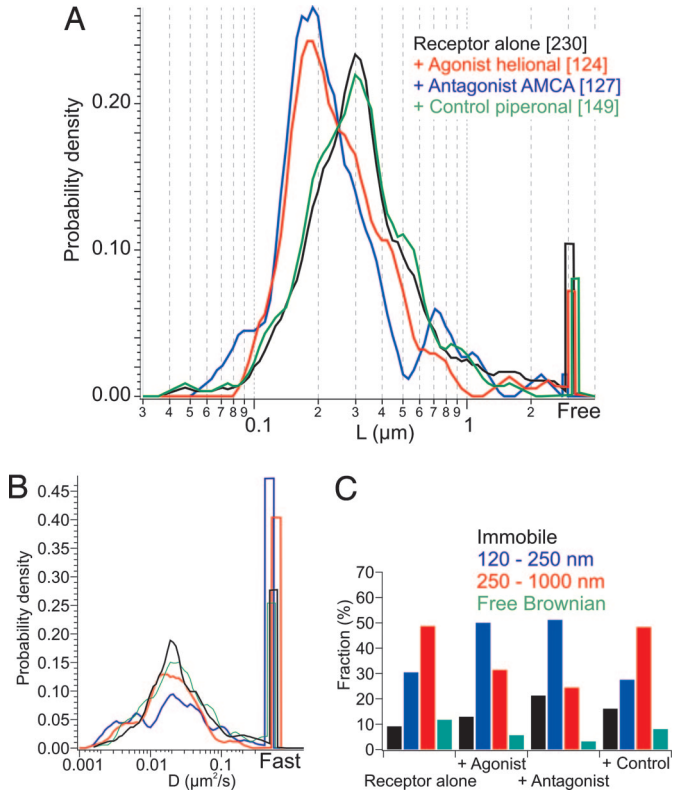

Fig. 5. Mobility of ORs. (*A*) Distribution of domain size *L* and diffusion coefficient *D*. (*B*) Number of receptors analyzed (shown in square brackets in *A*). (*C*) Classification of trajectories into four categories in the presence and absence of ligands.

into these four classes was supported by a cumulative analysis of the data separately for each class (23) revealing that a single diffusive component is contained in each class. By using this classification, we found 9 ± 4% (mean ± 95% confidence interval) of Cy5-labeled ACP-OR17-40 to be immobile, 12 ± 4% to be free, 30 ± 6% to be in small domains of 190 ± 10 nm, and 49 ± 7% to be in large domains of 300–550 nm. The molecules usually remained confined inside one domain during the whole observation time (2–10 s); hopping from one compartment to another was not observed.

Ligand-Induced Confinement of OR17-40s in Small Domains. The effect of ligand binding on the lateral diffusion of OR17-40 was investigated by adding either 200 μM of the agonist helional or 300 μM of the antagonist AMCA to cells expressing Cy5-labeled ACP-OR17-40. The distribution of the diffusion coefficients after addition of either compound did not differ greatly from that obtained for the unliganded receptor (Fig. 5*B*). Nevertheless, the principal population without ligand decreased in favor of a second, new contribution of very slow receptors ($D \approx 3 \times 10^{-3}$ μm²/s). This effect was similar for both ligands but stronger for AMCA. Even more pronounced, the domain size distribution changed significantly in a compound-specific manner (Fig. 5*A*). The population around $L = 190$ nm increased for both ligands but more strongly for the antagonist, which overall lead to a stronger confinement and immobilization of the receptor. Conversely, the main population around $L = 300$ nm decreased for both ligands, again more strongly for AMCA. The freely diffusing fraction remained unchanged in the presence of agonist (compared with its absence), but vanished almost completely in the presence of antagonist.

In summary (Fig. 5*C*), the fraction of OR confined to small domains increased significantly from 30 ± 6% to 50 ± 9% upon agonist addition, and even up to 51 ± 9% in the presence of antagonist, whereas the fraction of OR confined to large domains decreased from 49 ± 7% to 31 ± 8% for the agonist and to 24 ± 8% for the antagonist (χ^2 test: $P < 0.001$ in all cases). To ensure that this effect was specifically due to binding of the ligand and not to any unspecific effect of the ligand on the lipid membrane, the diffusion of ACP-OR17-40 was monitored after addition of 300 μM piperonal, a compound structurally similar to the agonist but that does not bind to the receptor (11). All fractions stayed constant upon addition of piperonal (28 ± 7% for the small confined fraction and 48 ± 8% for the large confined fraction). Careful comparison of $P(L)$ with and without piperonal (Fig. 5*A*) reveals the same three-component distribution with peaks at ≈190, 300, and 550 nm, respectively. This observation confirms our early hypothesis that ORs indeed are diffusing inside domains of at least three different specific sizes.

Discussion

The dual tagging of OR17-40 did not alter its biological activity and provided a molecular tool for studying dynamic processes of OR biogenesis, trafficking, diffusion in the plasma membrane, and endocytosis in living cells. Based on the continuous visualization of the total receptor population by GFP and the selective fluorescence pulse labeling of the receptors that were functionally integrated in the plasma membrane, we obtained real-time insights into the life cycle of an OR.

While focusing on the intracellular biosynthesis of OR17-40, we discovered that at a high level of expression the receptor was retained in intracellular compartments and only a small fraction was translocated to the plasma membrane. The number of these cell surface ORs was larger in low- vs. high-expressing cells. In highly expressing cells, ORs did not exit the ER, possibly because of receptor self-aggregation. Previous studies on OR expression in the *odora* olfactory sensory neuron cell line proposed a model in which receptor trafficking is controlled at two regulatory checkpoints: first, at the exit from the ER, which is crucial in heterologous cells; and second, in a post-Golgi compartment where ORs are blocked in undifferentiated *odora* cells (8). Our results indicate that, in heterologous cells, the first checkpoint is critical but OR17-40 does not remain blocked at the second, because the receptor was visible at the cell surface only a few hours after being in the Golgi apparatus.

Constitutive Receptor Internalization. Selective fluorescence labeling of ORs on the cell surface allowed us to follow the trafficking of OR17-40 after its insertion in the plasma membrane. Interestingly, this showed that OR17-40 undergoes constitutive internalization even in the absence of an agonist. By cell treatment with hyperosmotic sucrose, we provided evidence that this endocytic process occurred along the clathrin-dependent pathway. Furthermore, the internalized receptors colocalized predominantly with transferrin-receptor-positive endosomes after 20–30 min, suggesting continuous recycling.

Although constitutive internalization in the absence of a ligand has been reported for several GPCRs (19, 24–28), to our knowledge no indication of this phenomenon has been provided for ORs. Our present results indicate that receptor internalization, which is an agonist-dependent process in the classical model of GPCR signaling, can also occur without G protein activation and suggest that GPCRs can adopt many more conformational states than is usually believed (29).

We have shown that the receptor concentration at the cell surface remained constant upon addition of agonist or antagonist. Similar results were obtained for the human α1a-adrenergic receptor, for which very little variation in the level of constitutive internalization was observed upon addition of an agonist or an inverse agonist (19). Receptor trafficking away from and back to the plasma membrane are important to maintain a constant receptor density on the cell surface, especially in presence of an agonist, in order to retain

sensitivity to further ligand exposure (19, 21, 30). In this respect, constitutive internalization of the OR would help to maintain odor sensitivity over prolonged receptor stimulation.

The constitutive internalization of OR17-40 is unlikely to be caused by constitutive activation of the receptor or by exogenous ligands present in the culture medium or in the air, because the internalization is not blocked by antagonist treatment. This observation suggests that an endocytic motif might be responsible for targeting the receptor toward internalization. Studies on the thromboxane A_2 receptor indicated that a $YX_{2-3}\phi$ (where X is any amino acid and ϕ is a bulky hydrophobic amino acid) motif in the carboxyl tail of the receptor was responsible for the receptor's constitutive internalization (27). Although this specific motif is not present in the C-terminal part of OR17-40, it is possible that a different motif might play a similar role.

Lateral Membrane Diffusion of OR17-40. The specific pulse labeling of OR17-40 with a single photostable fluorophore allowed us to follow the diffusion of individual functional ORs on the cell surface by using single-molecule microscopy. Even without ligand, the diffusion of OR17-40 was found to be very heterogeneous, with 12% of the receptors diffusing freely in the plasma membrane, 9% being immobile, 30% diffusing inside small domains, and 49% diffusing inside larger domains. The broad distribution (2 decades) of diffusion coefficients exhibits a single population centered at 0.02 $\mu m^2/s$, a value that is typical for many transmembrane receptors (16, 31, 32). Diffusion coefficients of $\approx$0.1 $\mu m^2/s$, measured by fluorescence recovery after photobleaching, have been reported for several GPCRs (33–35). In contrast, the majority of OR40-17 has a slower diffusion coefficient, which could be the result of transient binding of the receptor to more immobile protein complexes, such as clathrin-coated structures.

The distribution of confinement sizes is slightly more complex, with a major population of $\approx$300 nm and two secondary populations of $\approx$190 and $\approx$550 nm. Monte Carlo computer simulations under realistic experimental conditions to estimate the shot-noise-limited width of the measured distributions ($\Delta\log(L) = 0.2$ decades FWHM) are described in *Supporting Text* and Fig. 6, which are published as supporting information on the PNAS web site. Similar domain sizes have been found for NK2R in HEK293 cells (35): Fluorescence recovery after photobleaching experiments revealed domains of radius = 420 $\pm$ 80 nm without ligand and 170 $\pm$ 50 nm when agonist was bound. The larger domains could arise from confinement by a membrane–skeleton/cytoskeleton fence structure (32, 36) or from long-range protein interactions (31) and might represent a population average of the two larger compartments found here. Because OR17-40 is constitutively internalizing, the smaller domains are likely to correspond to precursors of clathrin-coated pits (35, 37). Several GPCRs have been shown to accumulate in preformed clathrin-coated domains upon activation (38–40), rather than nucleating new domains as was previously believed. It was also proposed that the receptors are targeted inside prepits that are still flat and which invaginate following clathrin polymerization (40). Cezanne *et al.* (35) estimated from the radius of clathrin-coated pits of 75–100 nm that the radius of the corresponding flat domains measures between 150 and 200 nm, which corresponds well to the small domains of confinement found here for OR17-40.

The immobile receptors are probably in the process of internalization inside clathrin-coated pits (41). Receptors located inside clathrin-coated pits are thought to be tightly packed and immobile (36), and coated pits themselves are believed to be attached to the membrane skeleton, inasmuch as the formation of coated pits repeatedly occurs at defined sites of the plasma membrane (42).

Upon addition of either an agonist or an antagonist, the homogeneous yet broad distribution of OR17-40 diffusion coefficients became bimodal showing a new slow population. Under the same conditions, the strongly confined and immobile populations of receptors increased while the fraction inside the larger domains, and the freely diffusing fraction, decreased. Assuming that the small domains are precursors of clathrin-coated pits, the increase in the population of these domains would correspond to the receptors' recruitment to the pits and subsequent internalization. A similar restriction of receptor diffusion was found for the neurokinin receptors NK1R (43) and NK2R (35) after addition of an agonist. Why this also occurs for OR17-40 after antagonist addition is not entirely clear. An antagonist causing internalization was also found for the cholecystokinin receptor (44). It was postulated that the conformational change in the receptor induced or stabilized by the antagonist results in the unveiling of a domain that could promote receptor internalization. Similarly, our results suggest that the presence of a ligand (agonist or antagonist) inside the receptor-binding pocket is sufficient to promote the targeting of the receptor to precursors of clathrin-coated pits, even without receptor activation.

In conclusion, our results unravel mechanisms of internalization for OR17-40 that are very distinct from the standard model for GPCRs. First, ORs undergo continuous internalization and recycling, even in the absence of ligand. Second, the dynamics of this process are modulated by the binding of both classes of ligands: agonist and antagonist. These unique mechanisms of internalization might be instrumental in allowing for a rapid recovery of odor perception. They might also enable desensitization under the continuous presence of ligands, which usually remain bound to their receptors only for a very short time owing to their high binding constant in the micromolar range. Future comparative studies may reveal whether different ORs display different rate constants of internalization and turnover, providing an interesting potential mechanism for modulating olfactory perception.

By using ultrasensitive fluorescence microscopy, we were able to monitor the biogenesis, trafficking, membrane diffusion, and internalization of an OR down to the single-molecule level. We believe that novel labeling strategies to target specific subpopulations of proteins (45, 46), in combination with high-resolution microscopy and spectroscopy (47–50), will become increasingly important for live-cell proteomics.

Materials and Methods

Materials. DMEM, FCS, trypsine/EDTA, and Lipofectamine2000 were purchased from Invitrogen (Breda, The Netherlands), plasmids pECFP-ER and pECFP-Golgi from Clontech (Palo Alto, CA), transferrin-Alexa488 (Tf-Alexa488) from Molecular Probes (Eugene, OR), and sucrose from Sigma (Buchs, Switzerland).

OR17-40 cDNA was kindly provided by H. Hatt (Ruhr-Universität Bochum, Germany), clathrin-GFP cDNA by J. H. Keen (Kimmel Cancer Institute, Philadelphia, PA), CoA–Cy5 and AcpS by K. Johnsson (Laboratory for Photonics and Interfaces–ISIC, EPFL), and helional and AMCA by Firmenich (Geneva, Switzerland). CoA–CypHer was synthesized by A. Peer (Laboratory of Physical Chemistry of Polymers and Membranes–ISIC, EPFL).

Cell Culture, Plasmids, Transfection, and Labeling. HEK293 cells were used throughout. Experimental protocols are detailed in ref. 11. Plasmids of OR17-40 fusion proteins are described in *Supporting Text*. Cells stably or transiently expressing ACP-OR17-40 or ACP-OR17-40-GFP were labeled with 5 μM Cy5 or CypHer (1 μM AcpS/10 mM $MgCl_2$ in PBS) for 30 min at room temperature unless otherwise specified. Cells were then washed 3$\times$ with PBS.

Confocal Fluorescence Microscopy. Cells grown on 0.17-mm-thick glass coverslips were cotransfected with ACP-OR17-40-GFP cDNA and either pECFP-ER or pECFP-Golgi. At different times after transfection, samples were visualized by confocal microscopy (LSM510; Carl Zeiss Jena, Germany). Detection and distinction of the receptor (GFP) and the ECFP-ER or Golgi markers were achieved by appropriate filters in multitracking mode.

OR Internalization. The clathrin-dependent endocytic pathway was blocked by 10 min of incubation at 37°C with 0.45 M sucrose in PBS (17). Cells expressing ACP-OR17-40 were labeled with the pH-sensitive dye CoA–CypHer at 37°C, then washed 3× with PBS/sucrose and imaged on an in-house-fabricated fluorescence microscope.

For subcellular confocal colocalization with transferrin receptor, 50 μg/ml Tf-Alexa488 was added during labeling with CoA–CypHer. For colocalization with clathrin, cells stably expressing ACP-OR17-40 were transiently transfected with Clathrin-GFP cDNA and labeled with CoA–CypHer after 24 h.

To quantify the effect of agonist or antagonist binding on receptor internalization, cells transiently expressing ACP-OR17-40-GFP were incubated either overnight with the selective antagonist AMCA (300 μM), or 15 min and 1 h with the agonist helional (200 μM), and then labeled with CoA–Cy5 and immediately analyzed by FACS.

FACS Analysis. Cells expressing ACP-OR17-40-GFP labeled with CoA–Cy5 were diluted in PBS ($\approx 10^6$ cells per ml). FACS was done on a CyAn ADP LX 9 color analyzer (DakoCytomation, Fort Collins, CO) with 488-nm and 633-nm excitation. GFP fluorescence was detected in the green channel (530–540 nm) and the Cy5 signal in the red channel (665–720 nm). Data analysis (Summit; DakoCytomation) was selectively performed on viable cells by setting gates to exclude cellular debris.

Single-Molecule Microscopy. Cells stably expressing ACP-OR17-40 and grown on an eight-well chambered coverglass were labeled with 50 nM CoA–Cy5 and investigated on an in-house-fabricated epiluminescence wide-field microscope with 633-nm HeNe laser excitation and intensified CCD camera detection (50-ms exposure, 4-Hz frame rate) as described in refs. 16 and 51.

Diffusion of single receptors was analyzed with a custom-made single-particle tracking algorithm (16, 51). Briefly, fluorescence spots from single molecules are localized in an image series and fitted with a two-dimensional Gaussian (52). The positions in each frame were linked to obtain single-molecule trajectories. Mean square displacements, MSD(t_{lag}), were calculated for various time lags, t_{lag}, between two images for each molecule.

Visual inspection of the trajectories showed that most ORs appeared to be confined within domains of various sizes, whereas a few receptors diffused freely in the plasma membrane; directed motion was not observed. The apparent confinement might arise from the presence of membrane domains and/or from protein–protein interactions or immobile obstacles in the plasma membrane. Generally, protein or lipid trajectories on cell membranes are described by models for free diffusion, anomalous (sub-) diffusion, and confined diffusion (53). From traces limited in length by photobleaching to $\approx$20 observations, it is difficult to distinguish reliably different diffusion modes. Without preference for any particular model, phenomenologically, the evolution of MSD(t_{lag}) can be characterized by two parameters: an initial slope $\delta\mathrm{MSD}/\delta t_{lag}$ as $t_{lag} \to 0$ and a limiting MSD($t_{lag} \to \infty$), where free diffusion is included with MSD($t_{lag} \to \infty$) $\to \infty$. These two parameters are naturally incorporated in the model for confined diffusion: $\mathrm{MSD}(t_{lag}) = L^2/3\,[1 - \exp(-12Dt_{lag}/L^2)]$ as the diffusion coefficient D and the confinement size L, which we chose for the analysis of our data for this reason. A more detailed account of our considerations and the results when anomalous diffusion is assumed can be found in *Supporting Text* and Fig. 7, which are published as supporting information on the PNAS web site.

For some fast ($D > 0.5\ \mu\mathrm{m}^2/\mathrm{s}$) and confined molecules, the plateau of MSD(t_{lag}) was already reached at the first experimental data point at $t_{lag} = 250$ ms. In this case, only the domain size L was extracted, and D was arbitrarily set to $0.5\ \mu\mathrm{m}^2/\mathrm{s}$ solely to indicate this fact. Similarly, molecules with a very large diffusion range ($L > 3\ \mu$m) were considered to diffuse freely within the accessible area on the cell surface, and L was arbitrarily set to 3 μm for a better graphical representation. The planar projection recorded in single-particle tracking reflects the true trajectory only in an area of $\approx$3 μm diameter around the center of a cell. Outside this range, the cell boundary, and thus the membrane curvature, introduce a natural confinement not included in our model. Therefore, we corrected our data accordingly as just described.

We thank Dr. Andreas Peer for the synthesis of CoA–CypHer and Kai Johnsson for CoA–Cy5 and AcpS. This work was supported by grants from the Swiss National Foundation and the EPFL.

1. Buck L, Axel R (1991) *Cell* 65:175–187.
2. Bhandawat V, Reisert J, Yau KW (2005) *Science* 308:1931–1934.
3. Schwarzenbacher K, Fleischer J, Breer H (2005) *Histochem Cell Biol* 123:419–428.
4. Katada S, Tanaka M, Touhara K (2004) *J Neurochem* 90:1453–1463.
5. Ivic L, Zhang C, Zhang X, Yoon SO, Firestein S (2002) *J Neurobiol* 50:56–68.
6. Vargas G, Lucero MT (1999) *Chem Senses* 24:211–216.
7. Kajiya K, Inaki K, Tanaka M, Haga T, Kataoka H, Touhara K (2001) *J Neurosci* 21:6018–6025.
8. Gimelbrant AA, Haley SL, McClintock TS (2001) *J Biol Chem* 276:7285–7290.
9. Lu M, Echeverri F, Moyer BD (2003) *Traffic (Oxford, UK)* 4:416–433.
10. McClintock TS, Sammeta N (2003) *NeuroReport* 14:1547–1552.
11. Jacquier V, Pick H, Vogel H (2006) *J Neurochem* 97:537–544.
12. George N, Pick H, Vogel H, Johnsson N, Johnsson K (2004) *J Am Chem Soc* 126:8896–8897.
13. Meyer BH, Segura JM, Martinez KL, Hovius R, George N, Johnsson K, Vogel H (2006) *Proc Natl Acad Sci USA* 103:2138–2143.
14. Saito H, Kubota M, Roberts RW, Chi Q, Matsunami H (2004) *Cell* 119:679–691.
15. Adie EJ, Kalinka S, Smith L, Francis MJ, Marenghi A, Cooper ME, Briggs M, Michael NP, Milligan G, Game S (2002) *BioTechniques* 33:1152–1154,1156–1157.
16. Prummer M, Meyer BH, Francini R, Segura JM, George N, Johnsson K, Vogel H (2006) *ChemBioChem* 7:908–911.
17. Heuser JE, Anderson RG (1989) *J Cell Biol* 108:389–400.
18. Dale LB, Bhattacharya M, Seachrist JL, Anborgh PH, Ferguson SS (2001) *Mol Pharmacol* 60:1243–1253.
19. Morris DP, Price RR, Smith MP, Lei B, Schwinn DA (2004) *Mol Pharmacol* 66:843–854.
20. von Zastrow M, Kobilka B (1992) *J Biol Chem* 267:3530–3538.
21. Weber M, Blair E, Simpson CV, O'Hara M, Blackburn PE, Rot A, Graham GJ, Nibbs RJ (2004) *Mol Biol Cell* 15:2492–2508.
22. Destainville N, Salome L (2006) *Biophys J* 90:L17–L19.
23. Lommerse PH, Blab GA, Cognet L, Harms GS, Snaar-Jagalska BE, Spaink HP, Schmidt T (2004) *Biophys J* 86:609–616.
24. Roseberry AG, Hosey MM (1999) *J Biol Chem* 274:33671–33676.
25. Leterrier C, Bonnard D, Carrel D, Rossier J, Lenkei Z (2004) *J Biol Chem* 279:36013–36021.
26. Shapiro MJ, Trejo J, Zeng D, Coughlin SR (1996) *J Biol Chem* 271:32874–32880.
27. Parent JL, Labrecque P, Driss Rochdi M, Benovic JL (2001) *J Biol Chem* 276:7079–7085.
28. Xia S, Kjaer S, Zheng K, Hu PS, Bai L, Jia JY, Rigler R, Pramanik A, Xu T, Hokfelt T, Xu ZQ (2004) *Proc Natl Acad Sci USA* 101:15207–15212.
29. Whistler JL, Gerber BO, Meng EC, Baranski TJ, von Zastrow M, Bourne HR (2002) *Traffic (Oxford, UK)* 3:866–877.
30. Theriault C, Rochdi MD, Parent JL (2004) *Biochemistry* 43:5600–5607.
31. Daumas F, Destainville N, Millot C, Lopez A, Dean D, Salome L (2003) *Biophys J* 84:356–366.
32. Suzuki K, Ritchie K, Kajikawa E, Fujiwara T, Kusumi A (2005) *Biophys J* 88:3659–3680.
33. Barak LS, Ferguson SS, Zhang J, Martenson C, Meyer T, Caron MG (1997) *Mol Pharmacol* 51:177–184.
34. Horvat RD, Roess DA, Nelson SE, Barisas BG, Clay CM (2001) *Mol Endocrinol* 15:695–703.
35. Cezanne L, Lecat S, Lagane B, Millot C, Vollmer JY, Matthes H, Galzi JL, Lopez A (2004) *J Biol Chem* 279:45057–45067.
36. Sako Y, Kusumi A (1994) *J Cell Biol* 125:1251–1264.
37. Mousavi SA, Malerod L, Berg T, Kjeken R (2004) *Biochem J* 377:1–16.
38. Santini F, Gaidarov I, Keen JH (2002) *J Cell Biol* 156:665–676.
39. Scott MG, Benmerah A, Muntaner O, Marullo S (2002) *J Biol Chem* 277:3552–3559.
40. Merrifield CJ, Feldman ME, Wan L, Almers W (2002) *Nat Cell Biol* 4:691–698.
41. Cao TT, Mays RW, von Zastrow M (1998) *J Biol Chem* 273:24592–24602.
42. Gaidarov I, Santini F, Warren RA, Keen JH (1999) *Nat Cell Biol* 1:1–7.
43. Lill Y, Martinez KL, Lill MA, Meyer BH, Vogel H, Hecht B (2005) *ChemPhysChem* 6:1633–1640.
44. Roettger BF, Ghanekar D, Rao R, Toledo C, Yingling J, Pinon D, Miller LJ (1997) *Mol Pharmacol* 51:357–362.
45. Yin J, Lin AJ, Buckett PD, Wessling-Resnick M, Golan DE, Walsh CT (2005) *Chem Biol* 12:999–1006.
46. Hovius R, Meyer BH, Guignet EG, Vogel H (2006) in *Structural Genomics on Membrane Proteins*, ed Lundstrom KH (Taylor & Francis, Boca Raton, FL), pp 199–210.
47. Hell SW (2003) *Nat Biotechnol* 21:1347–1355.
48. Prummer M, Sick B, Renn A, Wild UP (2004) *Anal Chem* 76:1633–1640.
49. Jankevics H, Prummer M, Izewska P, Pick H, Leufgen K, Vogel H (2005) *Biochemistry* 44:11676–11683.
50. Bacia K, Kim SA, Schwille P (2006) *Nat Methods* 3:83–89.
51. Schreiter C, Gjoni M, Hovius R, Martinez KL, Segura JM, Vogel H (2005) *ChemBioChem* 6:2187–2194.
52. Schmidt T, Schutz GJ, Baumgartner W, Gruber HJ, Schindler H (1996) *Proc Natl Acad Sci USA* 93:2926–2929.
53. Saxton MJ, Jacobson K (1997) *Annu Rev Biophys Biomol Struct* 26:373–399.